Resistance Spot Welding of Aluminum Alloy to Steel with Transition Material — From Process to Performance — Part I: Experimental Study

Weld strength, failure mode, and fatigue life were compared with self-piercing rivets of the same dissimilar metals combination

BY X. SUN, E. V. STEPHENS, M. A. KHALEEL, H. SHAO, AND M. KIMCHI

ABSTRACT. This paper summarizes our work to date on resistance spot welding of aluminum alloy to steel, from process development to performance evaluation. Since aluminum alloys and steel cannot be readily fusion welded together due to their drastically different thermal physical properties, a cold-rolled clad material was introduced as a transition to aid the resistance welding process. The optimal welding parameters and electrode selections were established using experimental approaches.

The welded samples' mechanical behaviors were then evaluated using static and dynamic weld strength tests as well as cyclic fatigue tests. The weld strength, failure mode, and fatigue life were then compared with self-piercing rivets of the same dissimilar metals combination. Statistical analyses were also performed to analyze the effects of different failure modes on samples' peak strength and energy absorption.

Introduction

It is envisioned by the automotive industry that the optimized vehicle design in terms of performance and cost can only be achieved by using different materials at different vehicle locations to utilize the materials' functionalities to the fullest extent. Today, steel and aluminum are the most important construction materials for the mass production of automotive structures. It is well known that metallurgical bonds between aluminum and steel are difficult to achieve with fusion welding because of the inherent discrepancies in electrical, thermal, and mechanical properties between the two materials. For fusion welding processes such as direct resistance spot welding (RSW), little or no mutual solubility of aluminum and steel exists. The intermetallic compound that is formed between the two metals often results in cracking, brittleness, and susceptibility to corrosion.

The use of a transition material to facilitate spot welding of aluminum to steel is a concept that has shown promise in the past (Refs. 1–2). Use of this transition insert allows for two separate weld nuggets to be formed in their respective aluminum/aluminum and steel/steel interfaces. Joining at the aluminum/steel interface is achieved by the cold-clad process (Ref. 1). Few previous studies exist on this subject matter, and almost all of these studies focus on nugget growth kinetics for the spot welds using experimental approaches. There is a lack of understanding on the performance of these spot welds, particularly in comparison with other joining methods such as self-piercing rivets.

The first purpose of this study was to examine the possibility of using an intermediate, transition material to spot weld aluminum alloy to steel for structural applications. The optimal welding parameters and electrode selections were established using an iterative experimental approach. Welded samples were then fabricated using the optimized welding parameters. The welded samples' mechanical behaviors were then comprehensively evaluated using static and dynamic weld strength tests as well as cyclic fatigue tests under different loading configurations. The weld strength, failure mode, and fatigue life were then compared with self-piercing rivets of the same two dissimilar metals combination.

KEYWORDS

Spot Welding
Dissimilar Metals Joining
Aluminum Alloy
Transition Material
Aluminum-Clad Steel
Nugget Growth
Weld Strength
Weld Dynamic Strength
Weld Fatigue Strength

Welding Process Development

Material Selections

The dissimilar metals investigated in this study were 1.4-mm SAE1008 mild steel sheet and 2-mm 5182-O aluminum alloy sheet. The transition material introduced was a cold rolled clad material of aluminum to steel. Cold rolled cladding is a process that combines deformation and surface coating. The energy necessary for the coating process is obtained almost exclusively from the deformation process. Compared to the competing processes of electro- or hot-dipped coatings, strips can receive thick coating layers in a very short time. Because of low heat input, the formation of alloyed intermetallic layers can be suppressed at the interface of the clad materials. The metals are bonded together by extremely high pressure, which results in deformation at the interface (Ref. 1). The percentage of the coating is established by the thickness of the nonferrous metal strip related to the steel strip thickness.

Two total thicknesses of the transition materials were investigated in this study: 1.0 and 1.5 mm. The aluminum/steel ratios are 20/80 for the two thicknesses, meaning that the ratio of aluminum thickness vs. entire sheet thickness is 20%. The aluminum in the transition material is a 1050 alloy with low Si content and high aluminum purity. The steel in the transition material is an aluminum-free, low-carbon steel equivalent to SAE1006 steel. The

X. SUN is with Battelle Memorial Institute, Columbus, Ohio. E. V. STEPHENS and M. A. KHALEEL are with Pacific Northwest National Laboratory, Richland, Wash. H. SHAO and M. KIMCHI are with Edison Welding Institute, Columbus, Ohio.

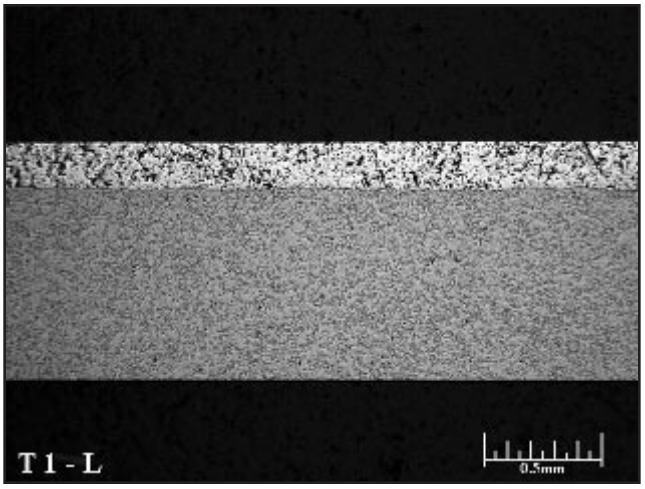

Fig. 1 — Cross section of the 1.0-mm-thick aluminum-clad steel sheet: the thickness of the aluminum layer is 0.2 mm and the thickness of the steel layer is 0.8 mm.

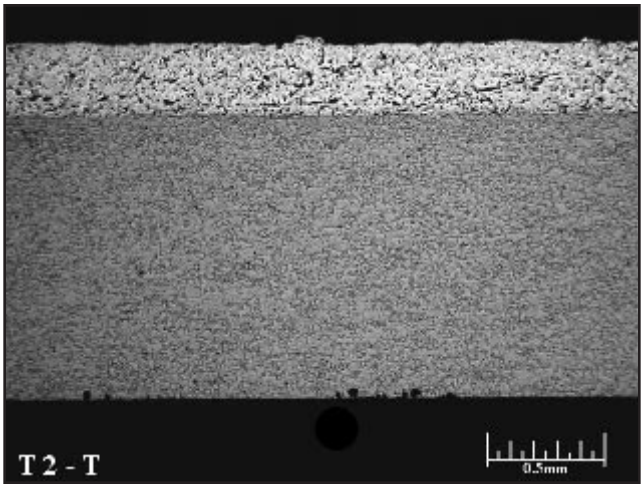

Fig. 2 — Cross section of the 1.5-mm-thick aluminum-clad steel sheet: the thickness of the aluminum layer is 0.3 mm, and the thickness of the steel layer is 1.2 mm.

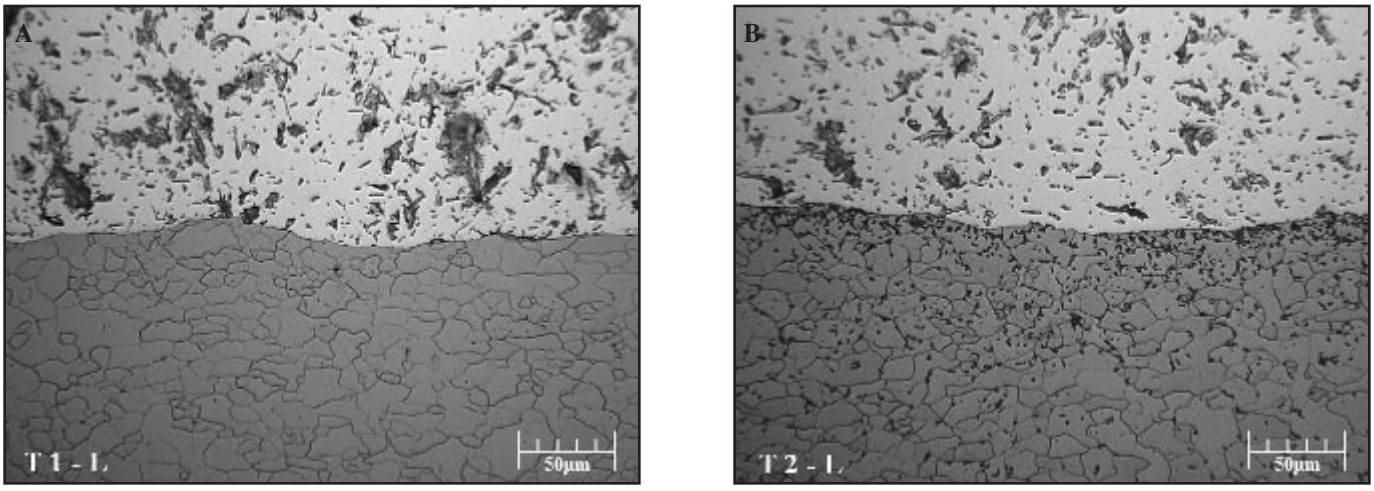

Fig. 3 —A — Aluminum/steel interface of the 1.0-mm-thick aluminum-clad steel sheet, with no intermetallic compound observed; B — aluminum/steel interface of the 1.5-mm-thick aluminum-clad steel sheet, with no intermetallic compound observed.

cross sections of these two aluminum-clad steel sheets are shown in Figs. 1 and 2. In Fig. 1, the clad sheet is 1.0 mm thick, in which the thickness of the aluminum layer is 0.2 mm, and the thickness of the steel layer is 0.8 mm. In Fig. 2, the clad sheet total thickness is 1.5 mm, with the thickness of the aluminum layer being 0.3 mm and the thickness of the steel layer being 1.2 mm. The interface bond structures of the two aluminum-clad steel sheets are shown in Figs. 3A and 3B, respectively. It appears that aluminum and steel are solid-state bonded, with no intermetallic compounds observed.

It should be noted that the clad ratio of 20% was not optimized for our particular resistance spot welding application. Because of the small amount of the transition material needed for this study, rolling of a clad strip with our desirable clad ratio was not economically feasible. The material with 20% clad ratio was adopted because of the on-shelf availability of the material supplier.

Electrode Selections

Welding trials were conducted on a single-phase 100-kVA pedestal-type Taylor-Winfield resistance welding machine equipped with a Medar MedWeld 3000s constant voltage controller. A fast follow-up welding head was used. In the initial stage of electrode selections, 1-mm transition material and the following initial welding parameters were used:

- Electrode force: 650 lb-f
- Welding current: 13.6 kA with 74% heat
- Welding time: 5 pulses of 7 cycles welding + 2 cycles holding

The following two combinations of electrode pairs were investigated experimentally:

- Combination No. 1 — Both sides: 30-deg truncated cone Class 2 electrodes with 8-mm face diameter and 3-in. face radius
- Combination No. 2 — Aluminum side: 30-deg truncated cone Class 2 electrode with 8-mm face diameter and 3-in. face radius; steel side: 30-deg truncated cone Class 2 electrode with 8-mm face diameter and flat faced.

Combination No. 1 is the type of electrode recommended by Ford Motor Company for aluminum spot welding (Ref. 12). During our initial welding trials with electrode combination No. 1, frequent expulsion was observed. In addition, a ring of softened aluminum was observed being squeezed out from the nugget periphery and forming a collar of aluminum outside the nugget area on the aluminum/aluminum faying interface, which further aggravated the final sheet separation. Based on these observations, electrode combination No. 2 was chosen by machining out the radius portion of the electrode tip on

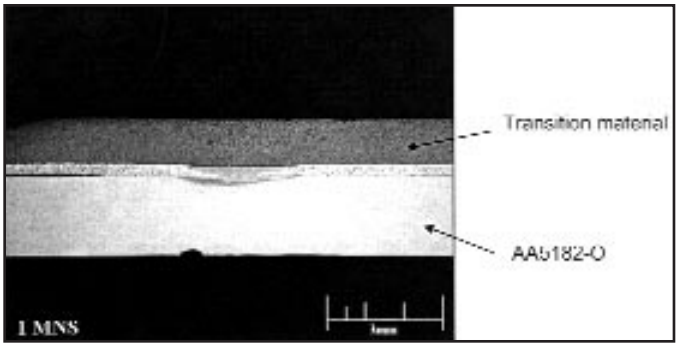

Fig. 4 — Weld cross section at 4 cycles weld time: no melting observed. The steel sheet separated from the transition sheet due to short weld time.

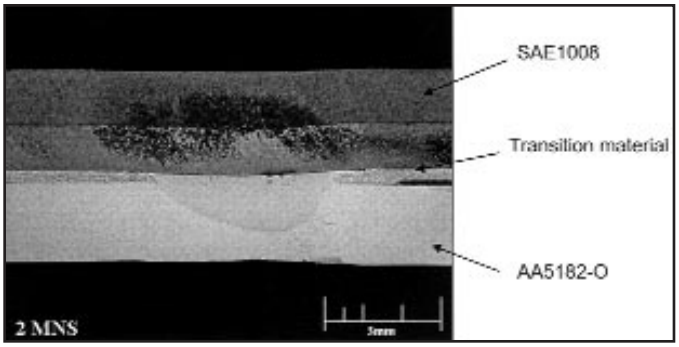

Fig. 5 — Weld cross section at 8 cycles weld time: initial melting observed.

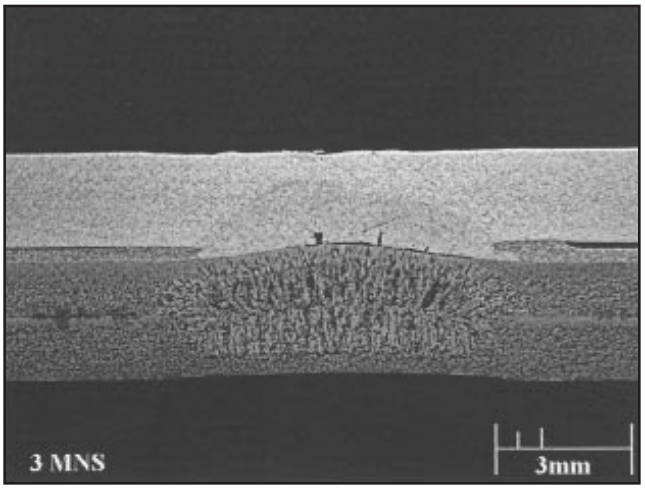

Fig. 6 — Weld cross section at 12 cycles weld time (1st pulse).

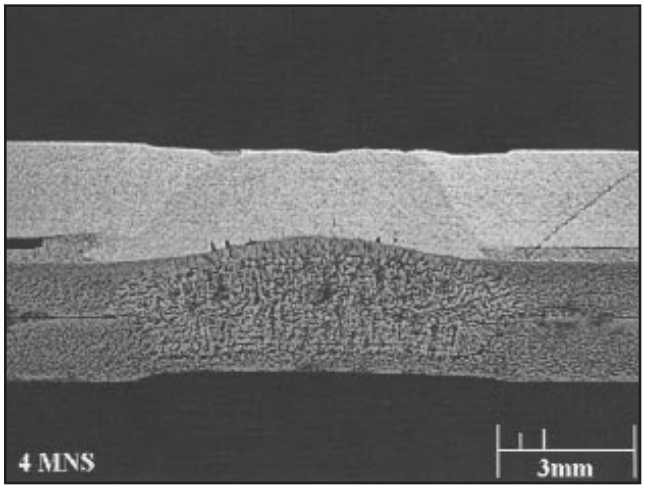

Fig. 7 — Weld cross section for (1st pulse) + (4-cycle current on).

the steel side. Further welding trials with this pair of electrodes yielded better welds in terms of weld expulsion and sheet separation. Electrode combination No. 2 was then chosen for the rest of the study. Coupled electrical-thermal-mechanical finite element modeling procedures (Refs. 3–5) were also used in selecting the final electrode combinations. Those results will be discussed in Part II of our study.

Welding Parameter Selections

With the selected electrode combination, optimal welding parameters were determined by iterative welding trials. Both 1.0- and 1.5-mm transition materials were used. Peel and lap-shear tensile tests were used to provide a quick estimate of the weld quality. The results of the peel tests indicated that a weld button was easily achieved when peeling was conducted between the steel sheet and the transition material. However, it was extremely difficult to obtain a consistent full button pullout when peeling was conducted between the transition material and the aluminum sheet, even for the samples made with the same welding parameters. Since the peel test results were inconsistent, lap-shear tensile tests were also used to evaluate the weld quality. It appeared that the welds with 1.5-mm transition material yielded higher tensile shear strength than the welds with 1.0-mm transition material. Therefore, 1.5-mm-thick transition material was selected to make the welded samples for further performance evaluations. After iterative welding trials, the following welding parameters were finalized for spot welding of 2-mm 5182-O to 1.4-mm SAE1008 with 1.5-mm-thick transition material:

- Electrode on Al side: 30-deg truncated cone Class 2 electrode with 8-mm face diameter and 3-in. face radius
- Electrode on steel side: 30-deg truncated cone Class 2 electrode with 8-mm diameter, flat faced
- Electrode force: 1050 lb-f
- Welding current: 13.6 kA with 97% heat
- Welding schedule: 3 pulses of 12 cycles welding + 3 cycles holding
- Cooling water flow rate: 1.75 gal/min

Nugget Development Study

With the final welding parameters selected, weld nugget development studies were conducted experimentally to get an in-depth, fundamental understanding of the heat generation and nugget formation sequence of the weld. This was accomplished by consecutively metallurgically cross-sectioning the weld for every four welding cycles. The resulting weld cross sections are shown in Figs. 4–12 with increasing weld times. The experimental nugget growth study was also accompanied by coupled finite element analysis on heat generation and nugget growth. In Part II of this study, we will use the experimental weld cross sections to compare with the finite element predictions.

Figure 4 shows the weld cross section at the end of the first four welding cycles. Melting has not occurred at this time and there are some degrees of material softening at the aluminum/aluminum interface. In fact, the SAE1008 sheet separated from the transition material after the electrode was removed at the end of the hold cycle. At the end of the 8th cycle weld time, initial melting on the aluminum/aluminum interface starts to take place and heat has been rapidly conducted to the AA5182-O side — Fig. 5. At the end of the

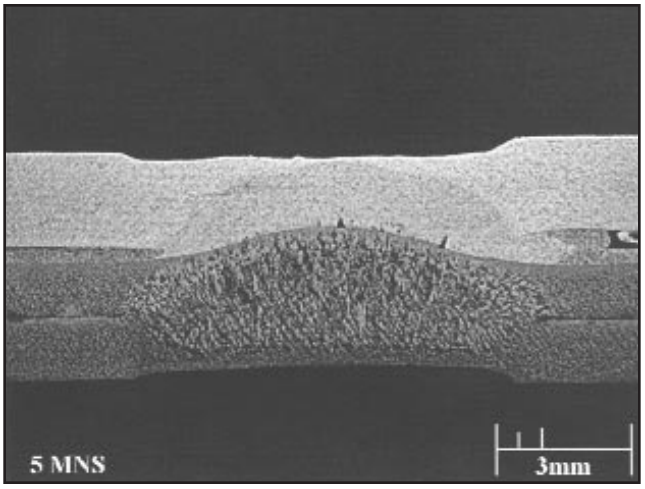

Fig. 8 — Weld cross section for (1st pulse) + (8-cycle current on).

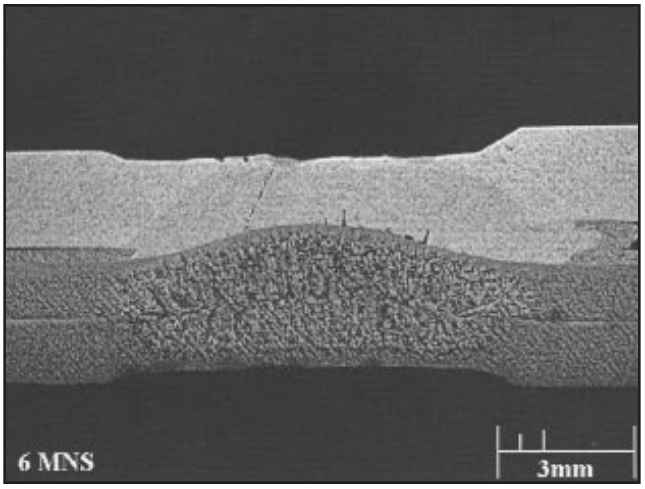

Fig. 9 — Weld cross section for (1st pulse) + (2nd pulse).

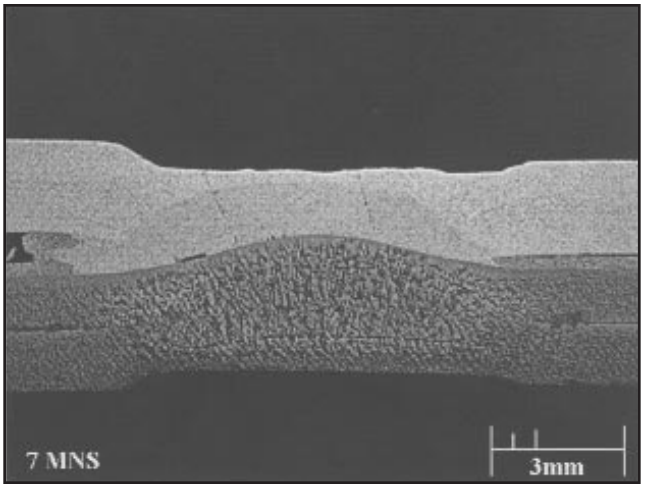

Fig. 10 — Weld cross section for (1st pulse) + (2nd pulse) + (4-cycle current on).

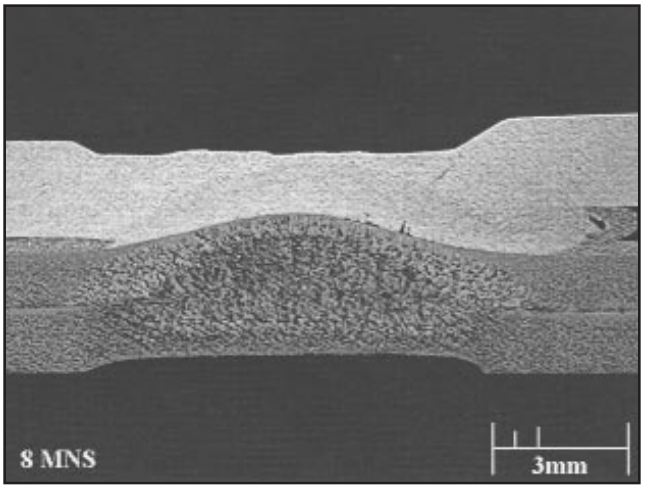

Fig. 11 — Weld cross section for (1st pulse) + (2nd pulse) + (8-cycle current on).

first welding pulse, shallow fusion zones can be observed on both the aluminum/aluminum interface and steel/steel interface as shown in Fig. 6. During the subsequent welding pulses, the width and depth of the fusion zones on the aluminum/aluminum side and steel/steel side continue to grow. At the end of the 3rd welding pulse, two distinct, well-developed fusion zones can be observed with some aluminum being pushed out on the aluminum/aluminum interface. The final nugget diameters on the aluminum side and the steel side are around 10.1 and 8.2 mm, respectively. It should be mentioned that the weld cross sections in Figs. 4–12 also show a slight degree of electrode misalignment during the welding process. The existence of electrode misalignment and the softened aluminum on the interface could be the reason for the one-sided material squeeze-out on the aluminum/aluminum interface as shown in Figs. 8–12.

Microstructure Evolution of the Aluminum/Steel Clad Interface during Welding

The microstructures of the aluminum/steel interfaces at the end of the 1st, 2nd, and 3rd pulses are presented in Figs. 13–15. Pores and gaps were observed at the steel/aluminum interface and in the aluminum side of the transition sheets. The presence of the weld discontinuities along the aluminum/steel interface can be attributed to the following factors: First, shrinkage stresses. During welding, the aluminum adjacent to the aluminum/steel interface is the last area to solidify. Shrinkage stresses (from solidification) combined with constraint from the surrounding solid metal can result in cavitations, typically evidenced as pores (adjacent to the steel) and solidification cracks (gaps). Secondly, they could be hydrogen-related porosities. This is similar to the hydrogen porosities that occur in arc welds and aluminum resistance spot welds. Since the aluminum surface is hydroscopic, it absorbs hydrogen from the atmosphere. During welding, this hydrogen is dissolved into the liquid metal. Upon solidification, the hydrogen is partitioned and therefore can form as gas or pores at the last area for aluminum to solidify.

Figures 13–15 also reveal the thickening of the intermetallic compound layer at the aluminum/steel interface within the transition material as the weld time progressed. During the first two welding pulses, the thickness of the intermetallic compound layer increased from 0 to about 7 μm. The thickness of the intermetallic layer increased to about 8.5 μm after the third welding pulse.

Peel tests conducted between the aluminum sheet and transition sheet indicated that interfacial failure often occurred at the aluminum/steel interface within the transition material, rather than the interface between the aluminum sheet

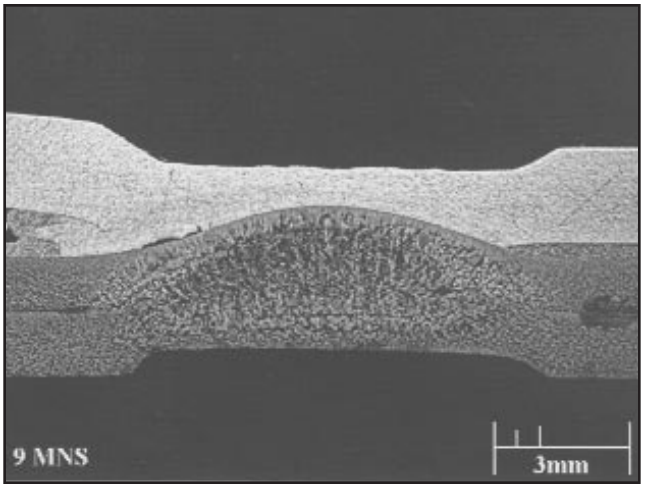

Fig. 12 — Weld cross section for (1st pulse) + (2nd pulse) + (3rd pulse).

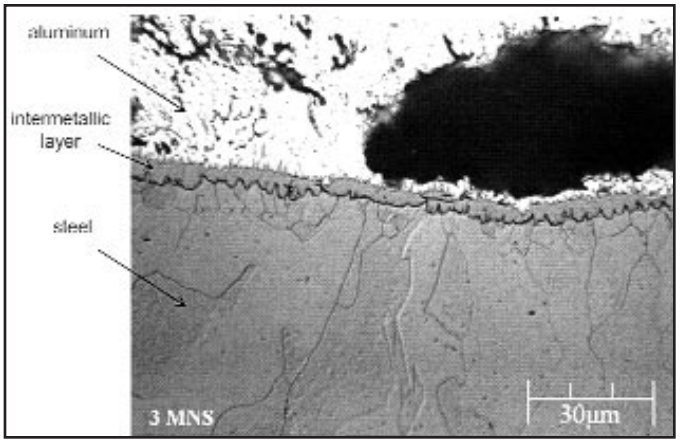

Fig. 13 — Microstructure of the aluminum/steel interface for the weld shown in Fig. 6, at the end of the 1st welding pulse.

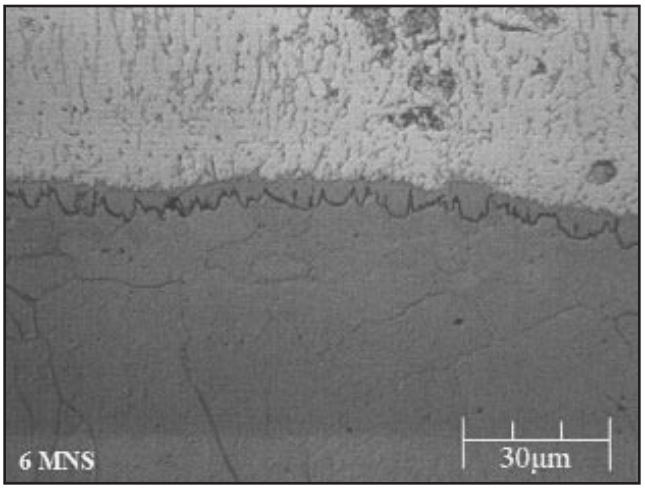

Fig. 14 — Microstructure of the aluminum/steel interface for the weld shown in Fig. 9, at the end of the 2nd welding pulse.

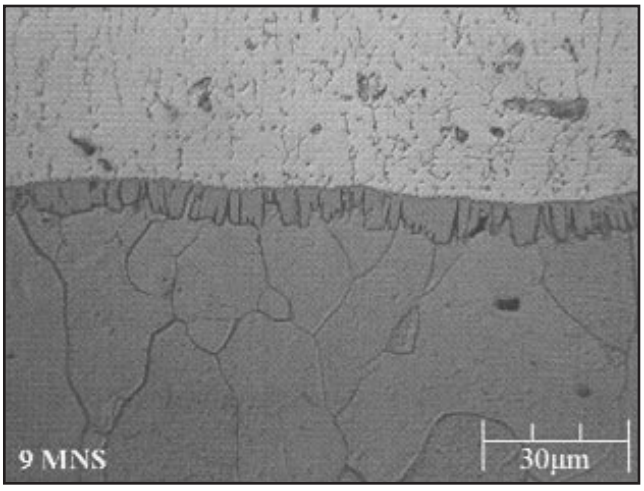

Fig. 15 — Microstructure of the aluminum/steel interface for the weld shown in Fig. 12, at the end of the 3rd welding pulse.

and the transition sheet. It is conceivable that the pores and gaps at the aluminum/steel interface could have provided the favorable fracture paths for peel test samples to fail at the interface. The presence of the brittle intermetallic compound layer at the aluminum/steel interface also contributes to such brittle interfacial failures. In general, the thicker the intermetallic layer, the more brittle the welds are and the less load and energy the welded sample will carry in the strength test. The effects of interfacial fracture on the welded samples' performance will be addressed in the next section.

As an interesting comparison, Fig. 16 shows the cross section of a spot weld made between 1-mm AA5052 and 0.8-mm bare low-carbon steel without any transition material. A semielliptical weld nugget is formed in the top aluminum sheet, and there is evidence of fusion material in the bottom steel sheet. However, a very thick layer of intermetallic compound formed on the faying interface with thickness around 65 μm. A recent study by Rathod and Kutsuna (Ref. 13) on joining of AA5052 and low-carbon steel concluded that with the increase of total thickness of the intermetallic layer, the amount of Al-rich intermetallic compound in it increases and the amount of Fe-rich intermetallic compound decreases. In addition, they also found that the amount of Al-rich brittle intermetallic compound on the interface drastically reduces the joint strength. Comparing the thickness of the intermetallic layers in Figs. 15 and 16, it is not difficult to conclude that the welds made with the transition material have a much thinner intermetallic layer and therefore will have much higher strength than the welds made without the transition material.

We should point out again that the cladding ratio of the transition material used in this study was not optimized. It is conceivable that, with thicker aluminum in the transition layer, an even thinner intermetallic layer can be achieved on the aluminum/steel interface during the welding process. Moreover, with thicker aluminum in the clad material, it will be more difficult for the fracture path to go through the aluminum layer and reach the aluminum/steel interface. Therefore, it would be more difficult for interfacial fracture to occur at the aluminum/steel interface during strength tests.

Dissimilar RSW Performance Evaluations

With the established welding schedule, welded samples were made for tensile shear (also known as lap shear), cross ten-

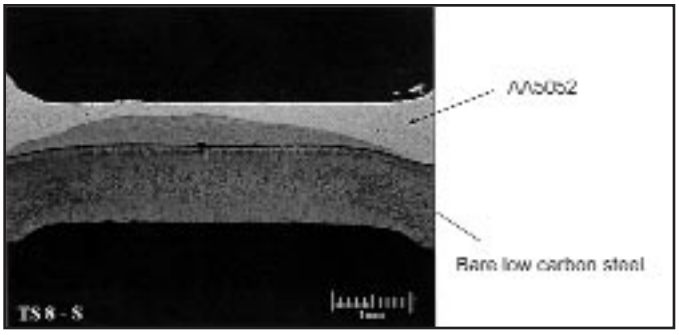

Fig. 16 — Cross section of 1-mm AA5052 to 0.8-mm bare low-carbon steel spot weld.

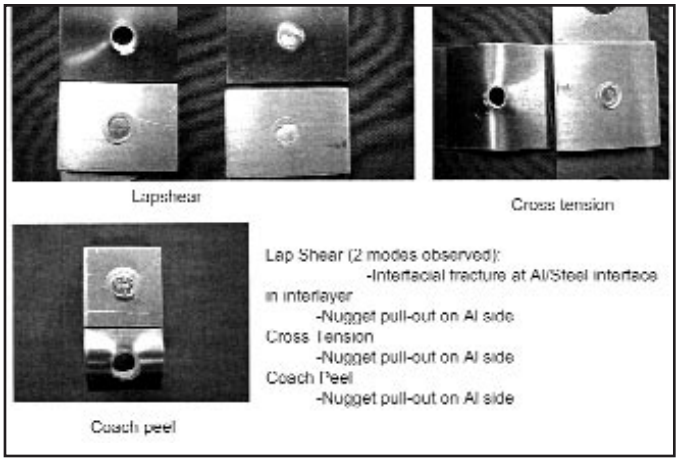

Fig. 17 — Illustration of different failure modes under different loading conditions.

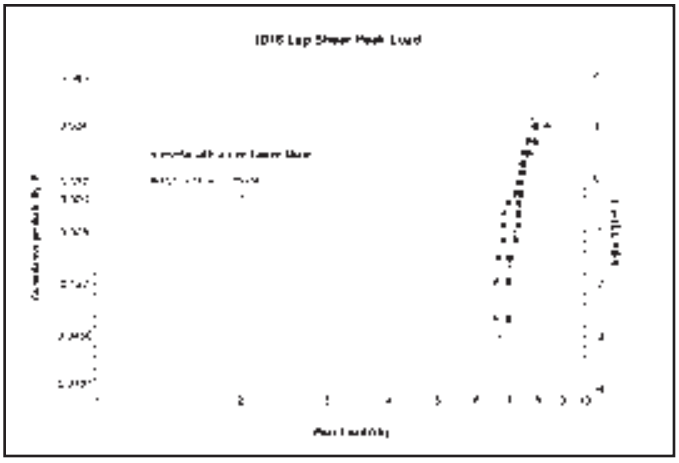

Fig. 18 — Dissimilar RSW population: peak load distribution for interfacial fracture and nugget pullout under lap shear.

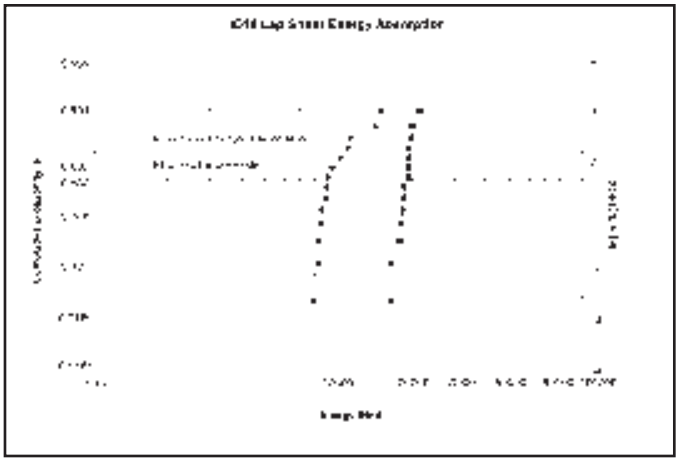

Fig. 19 — Dissimilar RSW population: distribution of energy absorption for interfacial fracture and nugget pullout under lap shear.

sion, and coach peel tests according to the coupon geometry developed in Ref. 6. Static, dynamic, and fatigue tests were then performed on the joint samples. In total, 30 quasi-static tests and ten dynamic tests were performed for each coupon configuration following the testing procedures described in Refs. 6 and 7.

Quasi-Static and Dynamic Performance Evaluations

For cross tension and coach peel samples, nugget pullout from the aluminum side was the consistent failure mode observed for both the static and dynamic samples tested — Fig. 17. For lap shear samples, however, a combination of interfacial fracture and nugget pullout from the aluminum side was observed for both the static and dynamic tests. The interfacial fracture mostly occurred at the aluminum/steel interface within the transition material, consistent with the observations in the peel tests as discussed in the previous section.

In order to study the effects of different failure modes on the peak load and energy absorption of the statically loaded lap shear samples, statistical analyses similar to those performed in Ref. 7 were conducted. Figure 18 shows the Weibull plots of peak load distributions for interfacial fracture and nugget pullout modes under static lap shear. It is clear that the modality and the mean values of these two failure modes for the static lap shear samples are close to each other, with the mean peak load for the interfacial fracture slightly lower than that for the nugget pullout. In other words, for this weld population, the samples' failure mode does not significantly influence their lap shear peak load. This observation is similar to the conclusions derived for aluminum spot welds in Ref. 7. However, the slope of the interfacial fracture curve is lower than that of the nugget pullout curve in Fig. 18; this is particularly true at low load levels. This observation indicates that the interfacial fracture mode has larger strength variation than the nugget pullout mode.

The statistical characteristics for the energy absorption of the two failure modes, as shown in Fig. 19, are drastically different. Energy absorption for nugget pullout mode fits perfectly on a Weibull paper, which indicates that it has a unique Weibull shape parameter and median value associated with this distribution. On the other hand, the energy absorption level for interfacial fracture has a bi-modal distribution. The mean energy absorption of the interfacial fracture population is only 52% of the mean energy absorption of the nugget pullout population. This is mainly due to the fact that for interfacial fracture mode, very little sheet bending takes place during the loading process. For nugget pullout mode, sheet bending caused by weld failure prolongs the total deformation of the failure event, resulting in increased total energy absorption.

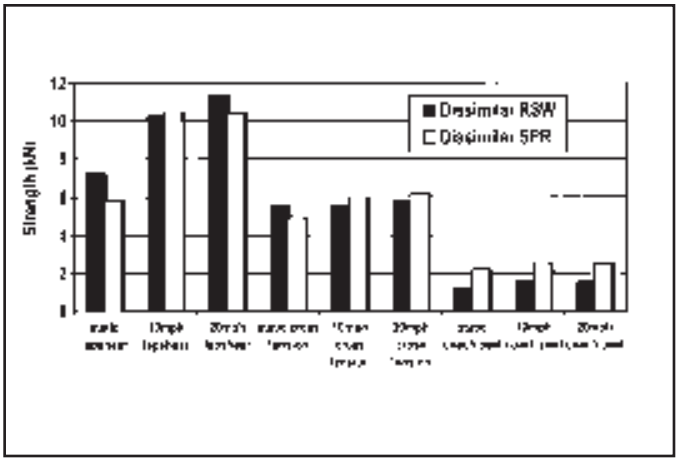

Fig. 20 — Comparison of peak load levels between dissimilar RSW and SPR.

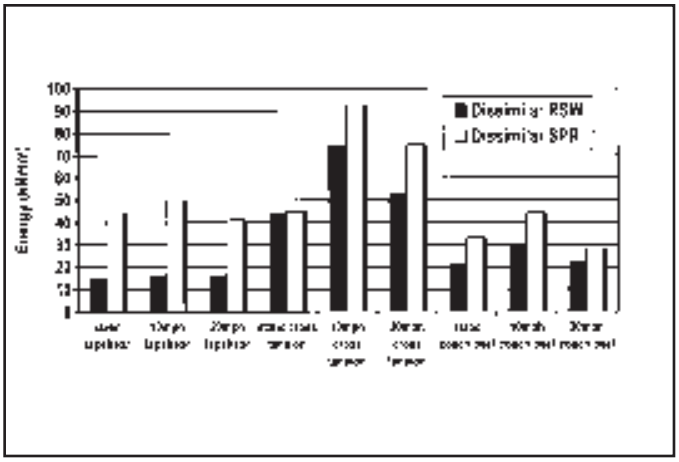

Fig. 21 — Comparison of energy levels between dissimilar RSW and SPR.

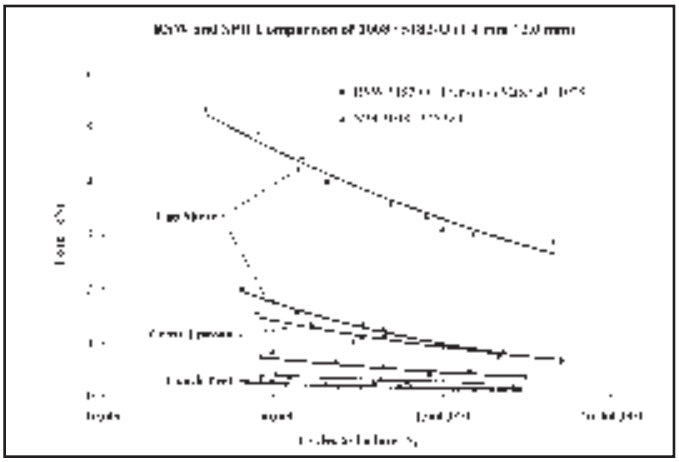

Fig. 22 — Fatigue life comparisons of dissimilar RSW and dissimilar SPR.

It is very important to note that the failure mode of a spot welded sample is greatly influenced by its weld attributes and the geometric configurations of the sample itself. Different analytical-based formulations have been developed in the literature to ensure nugget pullout mode of failure (Refs. 8 and 9). For example, a bending moment-based analytical equation was derived in Ref. 8 to predict the failure mode of a shear-loaded weld sample. Weld size and sheet thickness together with the ratio of the base metal tensile strength to the weld metal shear strength were used to determine the failure mode of the sample. Based on this theory and the assumption that the shear strength of the aluminum weld metal is about 0.7 times the tensile strength of the base metal (Ref. 14), the critical weld diameter for bending-type failure is calculated to be 7.8 mm for our lap shear samples with 50-mm coupon width. Since the final weld diameter on the aluminum side was ~10.1 mm, we should expect nugget pullout failure according to this prediction. However, as discussed earlier, both nugget pullout and interfacial fracture were observed in our static lap-shear test — Figs. 18, 19. The existence of pores and gaps on the aluminum/steel interface could have provided a favorable crack path and promoted interfacial fracture mode. Meanwhile, with many assumptions and simplifications employed in its derivation, the analytical prediction could have underestimated the critical weld diameter.

Comparison with Performance Data of Self-Piercing Rivets

Next, the static and dynamic performance data obtained for the dissimilar RSW population with transition material are compared with the performance data of the self-piercing rivet (SPR) population using the same two metal combinations: 2-mm AA5182-O (head side) to 1.4-mm SAE1008 (tail side). The dissimilar SPR population was fabricated by the Henrob Corporation with rivet head diameter of 7.5 mm, shank diameter of 5 mm, and length of 6.5 mm. A set of fabrication parameters was established for this SPR population and they are proprietary information of Henrob. The same coupon geometries as in the dissimilar RSW population (Ref. 6) were used for the dissimilar SPR population.

Overall, the static and dynamic strengths of the dissimilar RSW samples under lap shear and cross tension are comparable to those of the dissimilar SPR population — Fig. 20. Given the same material combinations, the strength levels for the RSW and SPR populations are primarily dependent on weld size, rivet geometry, and the corresponding failure modes. The failure modes for the lap shear and cross-tension SPR samples are all rivet head pullout from the AA5182-O side. Since the RSW population has slightly larger weld diameter than the SPR population, it should offer slightly higher static lap-shear and cross-tension strength. This is consistent with the experimental strength comparison shown in Fig. 20. Under coach peel condition, however, the peak load of the SPR population is higher than the RSW population because failure occurred at the tail end (SAE1008) of the rivet.

Comparison of total energy absorption between dissimilar RSW and dissimilar SPR is shown in Fig. 21. The energy absorption level of RSW under lap shear is considerably lower than those of SPR. This is because of the very low energy absorption level associated with the interfacial fracture mode of RSW. For SPR, on the other hand, all lap shear samples failed consistently in rivet head pullout mode. The energy absorption levels for RSW under cross-tension and coach peel loading conditions are slightly lower than those of SPR. Again, the energy absorption level for the RSW population can potentially be improved by using an optimized cladding ratio of the transition material to ensure nugget pullout failure during lap shear tests.

Comparisons of Fatigue Performance

Fatigue tests on lap shear, cross-

tension, and coach peel samples of the dissimilar RSW population were carried out using tension-tension ratio of R = 0.1. The results are shown in Fig. 22 in comparisons with the fatigue test results of the dissimilar SPR population.

The fatigue strength of the dissimilar SPR population is considerably higher than the RSW population. This observation is consistent with most of the reported data on fatigue strength comparisons between SPR and RSW (Ref. 10). The main reason for the superior fatigue behavior of rivets can be contributed to the fact that SPRs do not have the single-point crack tip (or notch tip) stress concentration effects as those in spot welds. In addition, the riveting process itself generates a compressive residual stress in the rivet periphery as opposed to the spot welding process, which generates yield-magnitude tensile residual stress at the weld periphery that is detrimental to the weld's fatigue performance (Refs. 5 and 11).

It should be pointed out again that the geometry of the weld sample makes a large contribution to the weld sample fatigue behavior. Figure 22 indicates that, for the same weld, the lap shear samples have the highest fatigue strength and the coach peel samples have the lowest fatigue strength. Many researchers have focused their efforts in addressing the coupon geometry effects using an equivalent stress intensity factor or structural stress approach (see, for example, Refs. 15 and 16). These approaches are very effective in comparing weld fatigue performance of sample populations made of different coupon configurations. The detailed fatigue performance comparisons for different joint populations using the equivalent stress intensity factor approach will be presented in a separate study.

Conclusions and Discussion

The objective of this research was to investigate whether spot welding between aluminum and steel can be achieved using a transition material. Experimental approaches were used in determining the optimal electrode combinations and welding parameters. Nugget formation process was then examined using consecutive metallurgical cross-sectioning. It was found that two distinct fusion zones formed during the spot welding process of aluminum to steel using a transition aluminum-clad steel strip. The nugget on the steel side is a regular, elliptical weld with dendritic grain structure inside the nugget region. The nugget on the aluminum side is the top half of the elliptical shape. Also, a thin, intermetallic compound formed on the aluminum/steel clad interface due to the welding heat input.

Static, dynamic, and fatigue performances of these welds were then examined and compared with the self-piercing rivet population of the same dissimilar materials combination. It was found that the static and dynamic strength of the RSW samples are comparable to those of the strength of the self-piercing rivets under the same loading conditions. However, because of different failure modes, the lap shear dissimilar RSW samples have a considerably lower energy absorption level than the dissimilar SPR samples. Fatigue strength comparison of the RSW population and the SPR population indicates that SPR population has much higher fatigue resistance than the spot welds.

This study demonstrated the spot weldability of aluminum to steel with transition clad material and evaluated the structural performance of these welds. The corrosion-related performance evaluation for the dissimilar RSW population is currently being pursued. It should be mentioned that the cladding ratio of the transition material used in this study was not optimized. With an optimized cladding ratio, it is conceivable that the weld static strength, failure mode, and energy absorption of the dissimilar RSW population can be further improved.

It should also be noted that the economic and production feasibilities of introducing such transition welds into automotive production need to be further studied and justified. First of all, spot welding using the transition material adds weight to the entire vehicle. Secondly, the relatively low yield of the cladding process would translate to the potential material cost increase for the automotive industry. Furthermore, the difference in thermal expansion coefficients of the two cladding materials would promote thermal distortion of the parts made of these materials. Nonetheless, the results of this study do suggest the potential application of aluminum clad steel as a load-bearing structural component as well as a material transition between the possible aluminum parts to the steel parts of the vehicle for optimized safety and weight reduction of a particular vehicle design.

Acknowledgments

Pacific Northwest National Laboratory is operated by Battelle for the U.S. Department of Energy under contract DE-AC06-76RL01830. This work was funded by the Dept. of Energy Office of FreedomCAR and Vehicle Technologies under the Automotive Lightweighting Materials Program managed by Dr. Joseph Carpenter. The USCAR program manager is James Quinn.

References

1. Johnson, J., Theile, R., and Kobeloer, N. 2000. Transition material- characteristics of aluminum-clad strip steels. *Proceedings of the IX Sheet Metal Welding Conference*, Detroit, Mich.

2. Chang, H. S., Johnson, G. F., Dickinson, D. W., and Tsai, C. L. 1999. Spot welding aluminum to steel — Transition material inserts help to overcome incompatibility. *Practical Welding Today*, May/June.

3. Sun, X. 2001. Effect of projection height on projection collapse and nugget formation — A finite element study. *Welding Journal* 80(9): 211-s to 216-s.

4. Sun, X. 2000. Modeling of projection welding processes using coupled finite element analyses. *Welding Journal* 79(9): 244-s to 251-s.

5. Sun, X., and Dong, P. 2000 Analysis of aluminum resistance spot welding processes using coupled finite element procedures. *Welding Journal* 79(8): 215-s to 221-s.

6. Vela, E., Sun, X., Davies, R., and Khaleel, M. A. 2002. Lap shear coupon design sensitivity study for self-piercing rivets and resistance spot welds. PNNL technical report for USCAR No. 13943, April.

7. Sun, X., Vela, E., Khaleel, M. A., and Davies, R. 2002. Effect of failure modes on strength of aluminum resistance spot welds. PNNL technical report for USCAR, October.

8. Koenigsberger, F. 1948. *Design for Welding in Mechanical Engineering.*

9. VandenBossche, D. J. Ultimate strength and failure mode of spot welds in high strength steels. Society of Automotive Engineers, paper No. 770214.

10. Booth, G. S., Olivier, C. A., Westgate, S. A., Liebrecht, F., and Braunling, S. Self-piercing riveted joints and resistance spot welded joints in steel and aluminum, SAE paper No. 2000-01-2681.

11. Bae, D. H., Sohn, I. S., and Hong, J. K. 2003. Assessing the effects of residual stresses on the fatigue strength of spot welds. *Welding Journal* 82(1): 18-s to 22-s..

12. Ford Laboratory Test Method BA 113-07: *Welding Acceptance Test for Aluminum*.

13. Rathod, M. J., and Kutsuna, M., 2004. Joining of aluminum Alloy 5052 and low-carbon steel by laser roll welding. *Welding Journal* 83(1): 16-s to 26-s.

14. *Metals Handbook*, Ninth Edition, Vol. 1, Properties and Selection: Irons and Steels. 1978. ASM International, Metals Park, Ohio.

15. Zhang, S. 2001. Fracture mechanics solutions to spot welds. *International Journal of Fracture* 112: 247–274.

16. Sheppard, S. D. 1995. Further refinement of a methodology for fatigue life estimation in resistance spot welds. ASTM STP 1292, *Advances in Fatigue Lifetime Prediction Techniques*. M. R. Mitchell and R.W. Landgraf, eds., pp. 265–282.